RSC Advances

PAPER

View Article Online
View Journal | View Issue

Cite this: *RSC Adv.*, 2014, **4**, 30035

Effect of carbonate anions on Bi-doped $Ca_2Ru_2O_7$ pyrochlores that are potential cathode catalysts for low temperature carbonate fuel cells

Cathryn A. Hancock,* Ai Lien Ong and John R. Varcoe

Received 2nd May 2014
Accepted 20th June 2014

DOI: 10.1039/c4ra05319b

www.rsc.org/advances

This *ex situ* electrochemical study investigates how the oxygen reduction reaction (ORR) on Bi-doped $Ca_2Ru_2O_7$ pyrochlore catalysts is affected by the addition of carbonate to the aqueous KOH (1 mol dm^{-3}) electrolyte. The parent $Ca_2Ru_2O_7$ catalyst has been previously reported to be selective towards the generation of CO_3^{2-} on the reaction of O_2 with CO_2 (in the presence of H_2O) at the cathode of low temperature alkaline polymer electrolyte fuel cells containing alkaline anion-exchange membranes (AAEM): a target is to develop low temperature carbonate fuel cells involving CO_3^{2-} conduction through the AAEM (for potential CO_2 utilisation). Rotating ring disk electrode (RRDE) voltammetry was used to probe the ORR behaviours of $Ca_2Ru_{2-x}Bi_xO_{7-y}$ catalysts with $x = 0.25$, 0.5, 0.75, and 1. The results show that as more Bi was doped into the pyrochlore catalysts, the poorer the on-set potentials compared to the parent $Ca_2Ru_2O_7$ (which itself yielded a poorer on-set potential to a benchmark Pt black catalyst). Higher levels of Bi-doping tended to reduce *n* values with higher levels of peroxide generated: all of the pyrochlore catalysts tested gave higher peroxide yields compared to the Pt black benchmark. However, the presence of CO_3^{2-} in the O_2-saturated KOH (1 mol dm^{-3}) electrolyte appeared to improve kinetic performance of the Bi-doped pyrochlore catalysts (the effect being greatest with the $x = 0.75$ catalyst).

Introduction

Fuel cell technology has many advantages compared to other energy generation/conversion techniques including higher efficiencies and potentially lower (local) emissions of greenhouse gases. There are many types of fuel cell with the proton-exchange membrane fuel cells (PEMFC) being the most widely known and developed low temperature option. However research on alkaline fuel cells (AFCs), including AFCs containing aqueous KOH electrolytes is still continuing due to the limitations of the PEMFCs, primarily the requirement for costly metal catalysts and poorer oxygen reduction reaction (ORR) kinetics at low pHs.[1–7] The use of alkaline polymer electrolyte fuel cells (APEFCs) promises to address many of the shortcomings of the PEMFCs by replacing the proton-exchange membrane with alkaline anion exchange membranes (AAEMs conduct anions such as OH^- and/or CO_3^{2-}).[8]

Traditional AFCs/APEFCs operate with OH^- cycles: however, an intriguing possibility is to operate APEFCs with CO_3^{2-} anion cycles, especially as there are reports that AAEMs can conduct CO_3^{2-} anions with reasonable conductivities of *ca.* 30 mS cm^{-1}.[9] The most debilitating aspect of using the OH^- cycles is the degradation of the AAEMs by the OH^- ions that are produced *via* the traditional ORR at the cathode (eqn (1)):

$$O_2 + 2H_2O + 4e^- \rightarrow 4OH^- \quad (1)$$

The OH^- anions are excellent nucleophiles and can displace the cationic head-groups of the AAEMs (commonly quaternary ammonium groups) *via* a multitude of degradation mechanisms.[10] An AAEM-containing CO_3^{2-} cycle system, as advocated by Kohl[11] and Mustain,[2] combats this by replacing the OH^- with less nucleophilic CO_3^{2-} (such that AAEMs that are unstable to OH^--containing electrolytes are chemically stable).[3–5] Using the CO_3^- cycle therefore increases the lifetime of the AAEM and may also improve the hydrogen oxidation reaction (HOR) kinetics at the anode.[4]

The challenge with developing a CO_3^{2-} cycle system is the need for an electrode which absorbs CO_2 in preference to water in order to generate CO_3^{2-} selectively over OH^- anions on reaction with O_2 at the cathode.[2–4,12,13] In addition to this, for the cathode catalyst to be effective in a low temperature carbonate fuel cell, it needs to have high electrical conductivity and electrochemical activity to facilitate the electron transfer processes and activate the O_2 double bond.[14–16] Currently only one CO_3^{2-} selective catalyst has been reported: the $Ca_2Ru_2O_7$ (Ru^V) pyrochlore.[2,4,13] The alkaline earth metal on the A site produces a catalyst with a high surface basicity: because CO_2 is a stronger Lewis acid than water, this leads to preferential absorption of

Department of Chemistry, Faculty of Engineering and Physical Sciences, University of Surrey, Guildford, GU5 0UW, UK. E-mail: cathrynhancock@hotmail.co.uk; Tel: +44 1483 686838

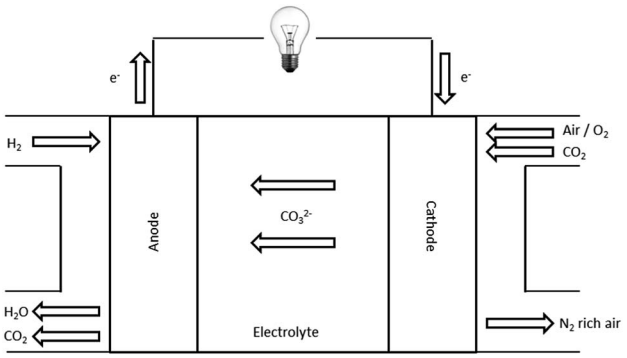

Fig. 1 Schematic for a low temperature carbonate fuel cell. Adapted from Mustain *et al.*[13]

CO_2. The B site introduces a metal with ORR activity in alkaline media, which in this case is Ru.

A low temperature carbonate fuel cell works as shown in Fig. 1. The CO_3^{2-} anions are produced from the selective reduction of O_2 and CO_2 at the cathode (eqn (2)). The CO_3^{2-} anions travel through the membrane (cathode → anode) where they oxidise the H_2 at the anode (eqn (3)).[11]

$$\text{Cathode: } 2CO_2 + O_2 + 4e^- \rightarrow 2CO_3^{2-} \quad (2)$$

$$\text{Anode: } 2H_2 + 2CO_3^{2-} \rightarrow 2H_2O + 2CO_2 + 4e^- \quad (3)$$

This initial study focuses on the synthesis of Bi-doped $Ca_2Ru_2O_7$ catalysts, which has been shown in other prior studies to have novel conductivity properties as well as thermal and chemical stability.[2,15,16] High surface area $Ca_2Ru_{2-x}Bi_xO_{7-y}$ (x = 0, 0.25, 0.5, 0.75 and 1) catalysts were synthesised to determine the effect that the much cheaper Bi (compared to Ru) has on the catalysts' performance and behaviour: this was probed using the rotating ring disk electrode (RRDE) hydrodynamic voltammetry.

Experimental

Synthesis and structural analysis

Most pyrochlore systems are synthesised using the standard solid state reaction of base oxides. However in this case, when the base oxides were reacted together, a calcium ruthenate perovskite, $CaRuO_3$ (Ru^{IV}), was produced instead of the target pyrochlore. The method used to produce this material was a reflux technique developed by Mustain *et al.*,[2] where the $KMnO_4$ was used as a replacement for oxygen in more traditional hydrothermal techniques. To begin with, an aqueous $KMnO_4$ (10 mmol dm^{-3}) solution was prepared by adding $KMnO_4$ (BDH) to a aqueous KOH solution (1 mol dm^{-3}, analytical grade, Fluka). CaO (BDH), $RuCl_3$ (Ru content 45–55%, Acros Organics) and Bi_2O_3 (99.999%, Sigma Aldrich) were then added to the solution in the correct ratios to produce $Ca_2Ru_{2-x}Bi_xO_{7-y}$ (x = 0, 0.25, 0.5, 0.75 and 1) and mixed thoroughly for 20 min at 80 °C. The solution was then refluxed at 200 °C for 24 h. Once cooled, the solution was filtered and washed with deionised water and heated overnight at 80 °C to dry. Powder X-ray diffraction (PANalytical Xpert Pro, λ = 1.5406 Å) was used to characterise the final catalysts. This technique was used to determine the phase purity of the materials as well as the structural properties of the system.

Catalyst ink and rotating ring-disk electrode (RRDE) preparation

The catalysts to be *ex situ* electrochemically tested were first ground into small particles using a pestle and mortar for 10 min. Once sufficiently ground, the catalyst (0.01 g) was suspended in deionised water (4 cm^3) and sonicated for 10 min. Propan-2-ol (1 cm^3) was then added followed by a further 10 min of sonication. Finally, Nafion 117 (20 μL of supplied dispersion [5% mass in lower aliphatic alcohols, Alfa Aesar]) was added to the ink mixture with a final sonication for 10 min. Before all procedures, the rotating Pt-ring glassy-carbon(GC)-disk RRDE (Ametek, UK, disk area = 0.2475 cm^2, ring inner diameter ∅ = 0.625 cm and ring outer diameter ∅ = 0.792 cm) was polished by gently moving in a figure of eight pattern on a Rayon Microcloth disk (Buehler) coated with an alumina slurry (particle size < 0.05 μm) and then thoroughly rinsed with deionised water. Before a 10 μL sample of the ink was pipetted onto the surface of the dry and clean RRDE, the catalyst ink was further sonicated for 10 min to ensure the ink was properly suspended. The inverted and catalysed RRDE was then spun at 600 rpm for 1 h at room temperature to dry the catalyst ink.

Electrochemical procedure

All RRDE electrochemical experiments were conducted using an IviumStat bipotentiostat (supplied by Alvatek, UK). This instrument also contained an internal impedance analyser. The instrument was controlled using IviumSoft software (ver. 1.831). The RRDE rotation rates were controlled using a Pine rotator (supplied by Ametek). The collection efficiency (N = the ratio of ring current to disk current) of the catalyst-free and freshly polished RRDE was determined by submerging in a solution of aqueous potassium ferricyanide ($K_3Fe(CN)_6$, 10 mmol dm^{-3}) in aqueous KCl (0.5 mol dm^{-3}) and sweeping the disk potential between 0.5 V and −0.5 V *vs.* Ag/AgCl (3 mol dm^{-3} NaCl internal solution) reference electrode at a sweep rate = 10 mV s^{-1}. The ring potential was set at 0.6 V *vs.* Ag/AgCl (3 mol dm^{-3} NaCl). N was measured for each RRDE rotation rate used. The RRDEs were submerged in deionised water for storage when not in use.

The electrolytes used for the RRDE ORR studies were a mixture of an aqueous solution of KOH (1 mol dm^{-3}, analytical grade, Fluka, used as supplied) and K_2CO_3 (Reagent grade, Fisher) in the following combination of concentrations: KOH (1 mol dm^{-3}) only [for blank experiments], KOH (1 mol dm^{-3}) + K_2CO_3 (0.01 mol dm^{-3}), KOH (1 mol dm^{-3}) + K_2CO_3 (0.05 mol dm^{-3}), and finally KOH (1 mol dm^{-3}) + K_2CO_3 (0.1 mol dm^{-3}). The electrolytes were purged with N_2 (99.999%, BOC) for 3 h to ensure the complete removal of CO_2 from the solution. Each solution was then separated into 90 cm^3 volume samples: one sample was purged with O_2 for 1 h to achieve O_2-saturation while the other solution was

kept O_2-free with continued purging with N_2. The limited current did not increase further with longer purging times, which indicated O_2 saturation was after 1 h of purging.

Once the electrolytes were fully oxygenated, a catalyst-free RRDE (as working electrode) was lowered into each electrolyte solution and the O_2 purge pipe was lifted so as to blanket the surface solution with O_2 [but not to mechanically disturb the solution (introduce unwanted convection)]. In addition, a reversible hydrogen electrode (Hydroflex RHE, Gaskatel) reference electrode and a Pt wire counter electrode (surface area significantly larger than the area of the RRDE working electrode: length = 50 cm and ∅ = 0.05 cm) were lowered into the solution. Immediately after immersion of the RRDE into each aqueous electrolyte under test, an impedance spectrum (frequency range 180 kHz to 96 Hz, voltage perturbation r.m.s. amplitude = 10 mV) was recorded to determine the uncompensated *iR*-correction. The background (catalyst-free RRDE) ORR testing was carried out by sweeping the disk potential from +1.00 to −0.30 V *vs.* RHE at 20 mV s^{-1}: the ring potential was held at +1.2 V *vs.* RHE at all rotation speeds used for catalyst testing (200, 400, 600, 800, 1200 and 1600 rpm).

Once the catalyst-free Pt-ring GC-disk RRDE was determined to be clean [having a low electron transfer number (n) in the above background tests], the catalyst to be tested was placed on the RRDE as discussed above. Impedance measurements were then repeated with each catalysed RRDE to determine the uncompensated *iR*-correction required for each test. Initially, cyclic voltammograms were recorded at 50 mV s^{-1} between the potential limits +1.2 and 0 V *vs.* RHE in the N_2 purged electrolytes for each catalysed RRDE. Following this, the catalysed RRDEs were then placed into the oxygenated electrolytes to perform the ORR measurements in a similar manner to the catalyst-free RRDE background tests: the reduction of O_2 was carried out by sweeping the disk potential from +1.00 to −0.30 V *vs.* RHE at 20 mV s^{-1}: the ring potential was held at +1.2 V *vs.* RHE. The measurements were repeated for each RRDE and electrolyte at 200 rpm until a stable response was obtained and then further ORR linear sweep voltammograms were recorded with increasing rotation speeds in the range 200–1600 rpm.

Results and discussion

Powder XRD characterisation

Fig. 2 shows the XRD patterns for the series of $Ca_2Ru_{2-x}Bi_xO_{7-y}$ ($x = 0$, 0.25, 0.5, 0.75, and 1). The structures were determined to be cubic with the space group $Fd\bar{3}m$ and with the unit cell parameters presented in Table 1. Peaks due to Bi_2O_3 impurities are present in the $x = 0.25$ and $x = 1$ catalysts with the latter highly doped sample containing extensive impurities [hence the unit cell parameters were estimated using the (222) peak at $2\theta = 30°$]. The broad peaks are indicative of small particle sizes but due to the extreme broadness for the $x = 0$ sample it was not possible to calculate the unit cell parameter: however, Sato *et al.* provide unit cell parameters of 10.197(2) with their more crystalline sample yielding sharper peaks (and more accurate cell parameter determinations).[17] Using this literature value, the cell volume increases on doping with Bi which is due to the increase in size of the Bi^{3+} ($r = 117$ pm, CN = 6) compared to the smaller Ru^{5+} ($r = 70.5$ pm, CN = 6).

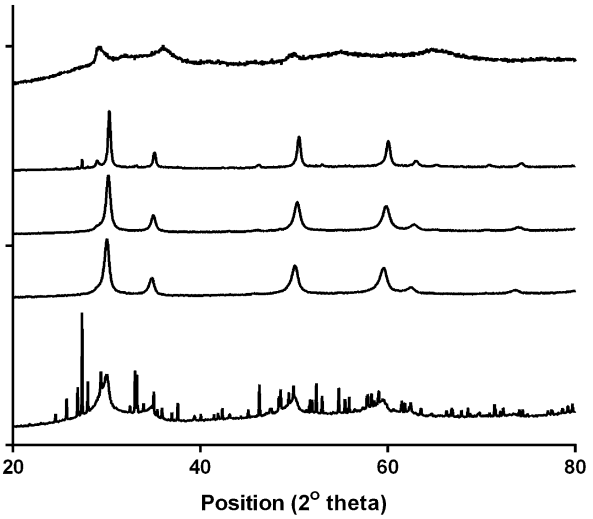

Fig. 2 Powder XRD profiles of the $Ca_2Ru_{1-x}Bi_xO_{7-y}$ catalysts synthesised. From top to bottom: $x = 0$, 0.25, 0.5, 0.75 and 1.

Table 1 The cell parameters of the catalysts (calculated from powder XRD data using the Unit Cell software) and particle sizes estimated using the Scherrer equation and the 222 peak

x	a/Å	Cell volume/Å^3	Particle size/nm
0	10.197[a]	1060.27[a]	—
0.25	10.2115(2)	1064.79(7)	25
0.5	10.2423(2)	1074.46(7)	25
0.75	10.2847(3)	1087.85(9)	27
1	10.3142[b]	1097.26[b]	18

[a] The cell parameters were taken from literature[17] due to the broadness of the XRD peaks. [b] The cell parameters were estimated from the (222) peak only due to the interferences from the impurities.

Cyclic voltammetry (CV)

As shown in Fig. 3, there are no significant changes in the peak potentials when CO_3^{2-} is added to the solution. For the undoped catalyst, the double layer region is wider when there is no CO_3^{2-} in the system. However with increasing amounts of Bi^{3+} dopant in the catalysts this trend reverses where the highest concentration of CO_3^{2-} yields the widest double layer.[18] This is an initial indication that the Bi^{3+} doped catalysts have a sensitivity to CO_3^{2-} anions. Additional features are seen in the CVs with the higher Bi content catalysts ($x = 0.75$ and $x = 1$): aqueous Bi^{3+}/Bi^{+} cations have reduction potentials in the range 0.2–0.5 *vs.* RHE. The impurities present may also be responsible, but it should be kept in mind that the $x = 0.25$ catalyst contained more impurities than the $x = 0.75$ according to the XRD profiles (but the latter contained more redox features in the CVs).

Calculation methods

Further investigations of the activities of the $Ca_2Ru_{1-x}Bi_xO_{7-y}$ catalysts for the ORR through the OH^- and CO_3^{2-} pathways

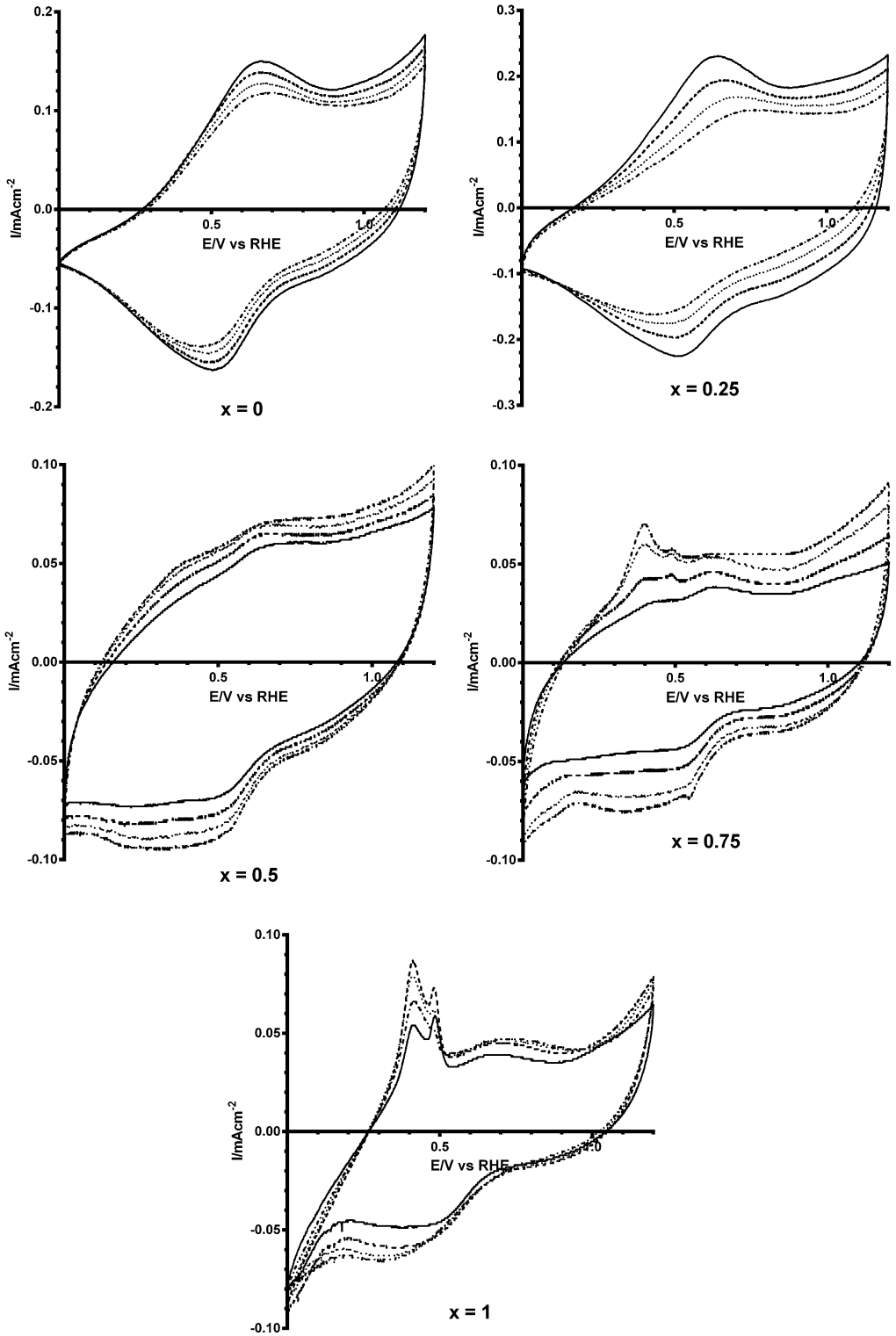

Fig. 3 Cyclic voltammograms of $Ca_2Ru_{2-x}Bi_xO_{7-y}$ ($x = 0$, 0.25, 0.5, 0.75 and 1) catalysts in N_2-saturated KOH: solid = no K_2CO_2 [KOH-only blank experiment], dashed = 0.01 mol dm^{-3}, dotted = 0.05 mol dm^{-3}, and dash-dot = 0.1 mol dm^{-3}.

were investigated using the RRDE technique. The RRDE technique was chosen over Koutecký–Levich analysis of RDE data as the method for determining the n value (the number of e^- reacting to reduce a single O_2 molecule). With the RRDE method, the n value can be determined from the ratio between the ring and the disk currents (after the collection efficiency has been determined). However, Koutecký–Levich and subsequent Tafel analysis of RDE data is dependent on knowing the exact

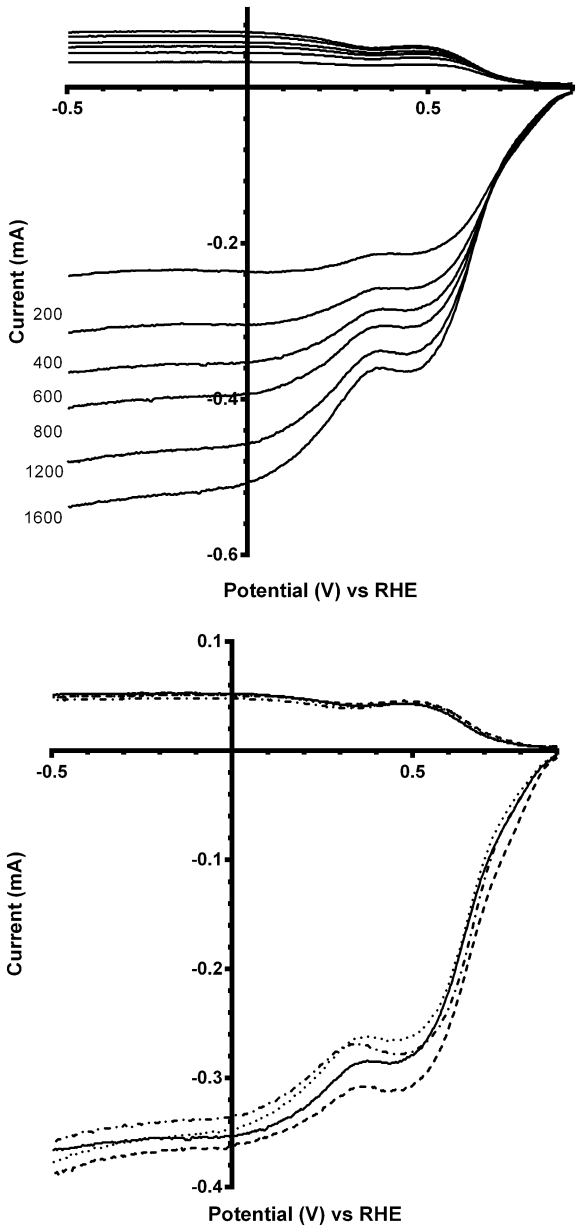

Fig. 4 RRDE linear sweep voltammograms (LSV) of $Ca_2Ru_2O_7$ in O_2-saturated aqueous KOH (1 mol dm^{-3}) at different scan rates (top) and O_2-saturated aqueous KOH (1 mol dm^{-3}) with varying concentrations of K_2CO_3 at 600 rpm (bottom): solid line = K_2CO_3-free, dashed = 0.01 mol dm^{-3}, dotted = 0.05 mol dm^{-3}, and dash-dot = 0.1 mol dm^{-3}.

properties of the solution (O_2 concentration, kinematic viscosity *etc.*), which will be problematic as: (a) it is time consuming to accurately measure the exact properties of each of the solutions, which will vary when different concentrations of CO_3^{2-} are added to the aqueous KOH (1 mol dm^{-3}); and (b) the exact electrochemical active surface areas of the catalyst are unknown (standard methods used for measuring electrochemical active surface areas for Pt/C catalysts cannot be directly translated into measuring this for catalysts such as those reported in this study). As will be shown later, n values obtained from Koutecký–Levich analyses are all higher with the Bi-doped catalysts compared to the n values calculated from the ratio of RRDE ring and disk currents (the preferred method in this study).

For the RRDE method of calculating the electron transfer number, n, it is necessary to determine the collection efficiency of the electrode being used. This is determined experimentally by measuring data using a well-known redox system: in this case the ferrocyanide–ferricyanide system was used (a simple reversible $n = 1$ e^- redox couple). This procedure to calculate collection efficiency has been performed extensively in the past: refer to Fig. 3 in ref. 19.

The (catalyst-free) Pt-ring GC-disk RRDE used in this study had an N value = 41%. N can then be used in eqn (4) and (5) along with the RRDE current data (at a potential of −0.3 V in these experiments) to determine the amount of HO_2^- yield (%) and the e^- (n) per O_2 for each catalyst and electrolyte:[20]

$$\%\text{peroxide} = \left(\frac{200 \times I_R}{N}\right) \Big/ \left(I_D + \frac{I_R}{N}\right) \quad (4)$$

$$n = \frac{4 \times I_D}{\left(I_D + \frac{I_R}{N}\right)} \quad (5)$$

Rotating ring-disk electrode (RRDE) voltammetry

Linear sweep voltammograms (LSV) were performed on all the catalysts in different electrolytes (containing different concentrations of CO_3^{2-}). Fig. 4 (top) shows the voltammogram at all rotation speeds for the parent catalyst $Ca_2Ru_2O_7$ in aqueous KOH (1 mol dm^{-3}). The inflections at *ca.* 0.3–0.5 V *vs.* RHE corresponds to the redox peaks observed in the cyclic voltammetry traces (Fig. 3) and are due to the reduction of Ru cations, which clearly introduces a second reduction wave. This redox peak feature is repeated with the Bi-doped catalysts. On addition of K_2CO_3 into the electrolyte, there were no significant

Table 2 Average e^- per O_2 reduction (n) and peroxide yields for the parent $Ca_2Ru_2O_7$ catalyst in O_2-saturated aqueous KOH (1 mol dm^{-3}) containing different concentrations of K_2CO_3

Concentration of K_2CO_3/mol dm^{-3}	n_{RRDE}[a]	Peroxide yield (%) from RRDE[a]	n_{K-L}[b]
0	2.97 ± 0.02	51.3 ± 1.0	2.14
0.01	3.03 ± 0.03	48.7 ± 1.0	3.45
0.05	2.95 ± 0.02	52.6 ± 1.1	3.13
0.1	2.98 ± 0.03	51.0 ± 1.2	3.12

[a] Arithmetic mean and sample standard deviations over all rotations rates. [b] Koutecký–Levich analyses conducted with the crude assumption that the addition of K_2CO_3 did not significantly alter the properties of the solution (*e.g.* O_2 solubility, kinematic viscosity *etc.*).

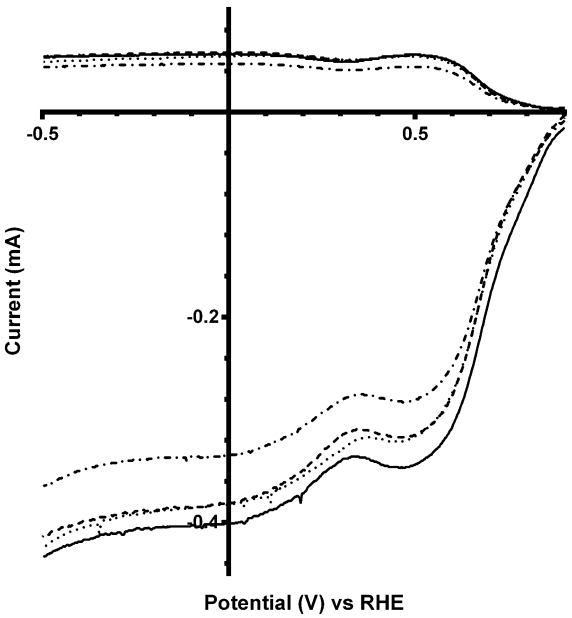

Fig. 5 RRDE LSVs of $Ca_2Ru_{1.75}Bi_{0.25}O_{6.75}$ in O_2-saturated aqueous KOH (1 mol dm^{-3}) and varying concentrations of K_2CO_3 at 600 rpm: solid line = K_2CO_3-free, dashed = 0.01 mol dm^{-3}, dotted = 0.05 mol dm^{-3}, and dash-dot = 0.1 mol dm^{-3}.

Table 3 Average n values and peroxide yields for $Ca_2Ru_{1.75}Bi_{0.25}O_{6.75}$ in O_2-saturated aqueous KOH (1 mol dm^{-3}) containing different concentrations of K_2CO_3[a]

Concentration of K_2CO_3/mol dm^{-3}	n_{RRDE}	Peroxide yield (%) from RRDE	n_{K-L}
0	3.02 ± 0.06	49.1 ± 2.8	3.79
0.01	2.97 ± 0.06	51.6 ± 3.0	4.01
0.05	3.06 ± 0.05	47.0 ± 2.4	3.90
0.1	3.03 ± 0.03	48.4 ± 1.2	3.27

[a] See footnotes to Table 2 for assumptions and the definition of errors.

changes in the form of the LSVs [Fig. 4 (bottom)] with the Bi-free parent catalyst: there was also no significant differences between the number of e^- per O_2 molecule reduction (n_{RRDE} in Table 2) and on-set potentials (the lowest concentration of K_2CO_3 [0.01 mol dm^{-3}] may even have led to a slightly improved on-set potential).

On doping with a small amount of Bi into the pyrochlore catalyst ($x = 0.25$), no significant difference in the n_{RRDE} values were observed on addition of CO_3^{2-} into the electrolyte (Fig. 5 and Table 3), while ORR on-set potentials were slightly shifted to less positive values (*i.e.* higher overpotentials). Both the on-set potentials and the n values were the same as the parent (Bi-free) catalyst for the K_2CO_3-free electrolyte (Fig. 6) indicating that a small level of Bi doping ($x = 0.25$) has no significant electrochemical effects. The parent compound has higher (more positive) ORR on-set potentials in the presence of CO_3^{2-} (0.1 mol dm^{-3}) compared to the $x = 0.25$ Bi-doped catalyst.

On addition of greater amounts of Bi with the $x = 0.5$ catalyst, there are visible shifts in the on-set potential to more

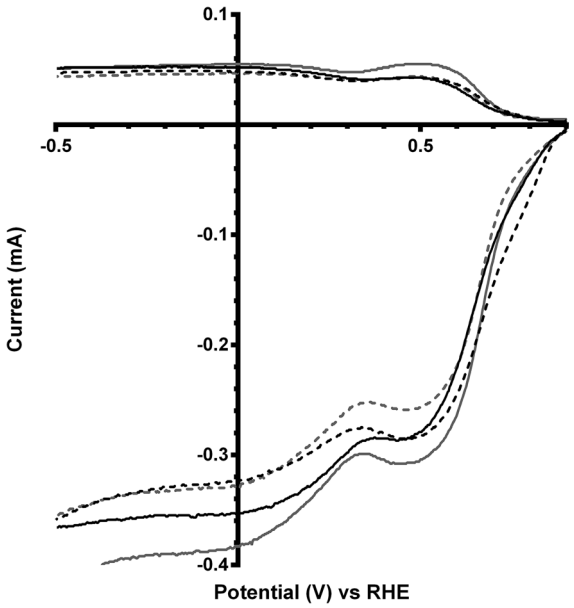

Fig. 6 RRDE LSVs of $Ca_2Ru_{2-x}Bi_xO_{7-y}$ ($x = 0$ in black and $x = 0.25$ in grey) in O_2-saturated aqueous KOH (1 mol dm^{-3}) containing the following concentrations of K_2CO_3: solid line = 0 mol dm^{-3} (CO_3^{2-}-free baseline) and dashed = 0.1 mol dm^{-3}. Rotation rate = 600 rpm.

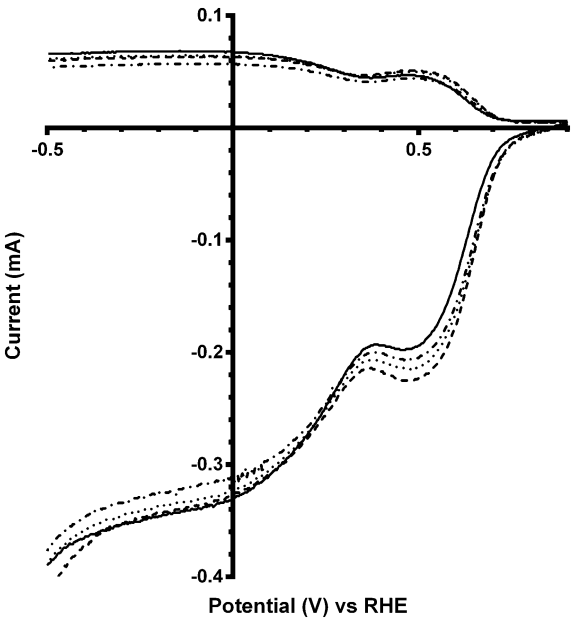

Fig. 7 RRDE LSVs of $Ca_2Ru_{1.5}Bi_{0.5}O_{6.5}$ in O_2-saturated aqueous KOH (1 mol dm^{-3}) and varying concentrations of K_2CO_3 at 600 rpm: solid line = K_2CO_3-free, dashed = 0.01 mol dm^{-3}, dotted = 0.05 mol dm^{-3}, and dash-dot = 0.1 mol dm^{-3}.

positive potentials on addition of CO_3^{2-} (*e.g.* Fig. 7). The on-set potentials remains at these more positive potentials with the continuing addition of K_2CO_3 in the electrolyte: this behaviour is different to the parent (Bi-free) system where only the addition of K_2CO_3 at the smallest 0.01 mol dm^{-3} concentration led to on-set potentials that were more positive compared to tests

Table 4 Average n values and peroxide yields for $Ca_2Ru_{1.5}Bi_{0.5}O_{6.5}$ in O_2-saturated aqueous KOH (1 mol dm^{-3}) containing different concentrations of K_2CO_3[a]

Concentration of K_2CO_3/mol dm^{-3}	n_{RRDE}	Peroxide yield (%) from RRDE	n_{K-L}
0	2.74 ± 0.02	62.9 ± 1.0	3.40
0.01	2.82 ± 0.02	59.1 ± 1.2	3.36
0.05	2.75 ± 0.03	61.2 ± 1.4	3.22
0.1	2.86 ± 0.04	57.1 ± 1.9	3.27

[a] See footnotes to Table 2 for assumptions and the definition of errors.

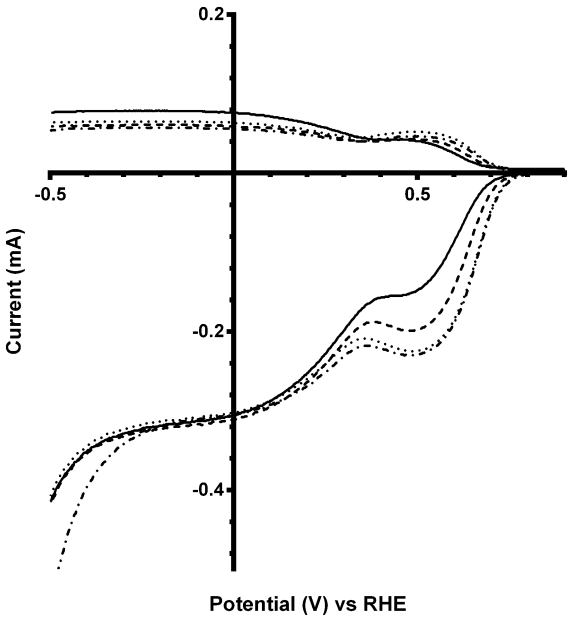

Fig. 8 RRDE LSVs of $Ca_2Ru_{1.25}Bi_{0.75}O_{6.25}$ in O_2-saturated aqueous KOH (1 mol dm^{-3}) and varying concentrations of K_2CO_3 at 600 rpm: solid line = K_2CO_3-free, dashed = 0.01 mol dm^{-3}, dotted = 0.05 mol dm^{-3}, and dash-dot = 0.1 mol dm^{-3}.

with the use of the K_2CO_3-free benchmark electrolyte. The n values were in general lower than with the Bi-free catalyst but, again, there is no significant increase in the n values with x = 0.5 Bi-doped catalysts on increasing concentrations of K_2CO_3 (Table 4).

These trends continue for $Ca_2Ru_{1.25}Bi_{0.75}O_{6.25}$ catalyst, which has the greatest shift in on-set potentials on addition of

Table 5 Average n values and peroxide yields for $Ca_2Ru_{1.25}Bi_{0.75}O_{6.25}$ in O_2-saturated aqueous KOH (1 mol dm^{-3}) containing different concentrations of K_2CO_3[a]

Concentration of K_2CO_3/mol dm^{-3}	n_{RRDE}	Peroxide yield (%) from RRDE	n_{K-L}
0	2.55 ± 0.02	72.7 ± 1.1	2.95
0.01	2.64 ± 0.04	68.0 ± 2.1	3.30
0.05	2.71 ± 0.02	64.7 ± 1.2	2.94
0.1	2.86 ± 0.05	57.0 ± 2.6	3.48

[a] See footnotes to Table 2 for assumptions and the definition of errors.

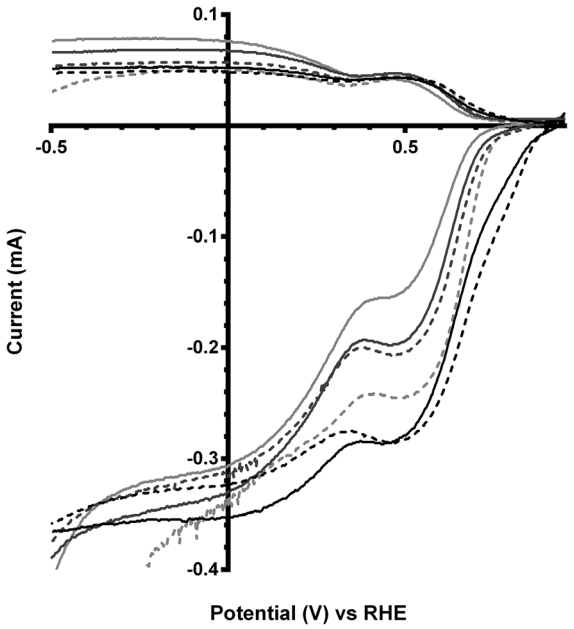

Fig. 9 RRDE LSVs of $Ca_2Ru_{2-x}Bi_xO_{7-y}$ (x = 0 in black, x = 0.5 in dark grey, and x = 0.75 in light grey) in O_2-saturated aqueous KOH (1 mol dm^{-3}) containing the following concentrations of K_2CO_3: solid line = 0 mol dm^{-3} (CO_3^{2-}-free baseline) and dashed = 0.1 mol dm^{-3}. Rotation rate = 600 rpm.

CO_3^{2-} into the electrolyte of all the catalysts studied (Fig. 8 and Table 5). The improvement in on-set potential on addition of CO_3^{2-} surpasses that of the prior x = 0.5 Bi-doped catalyst, which again suggests that higher concentrations of K_2CO_3 in the electrolyte can improve the performances of the higher Bi-

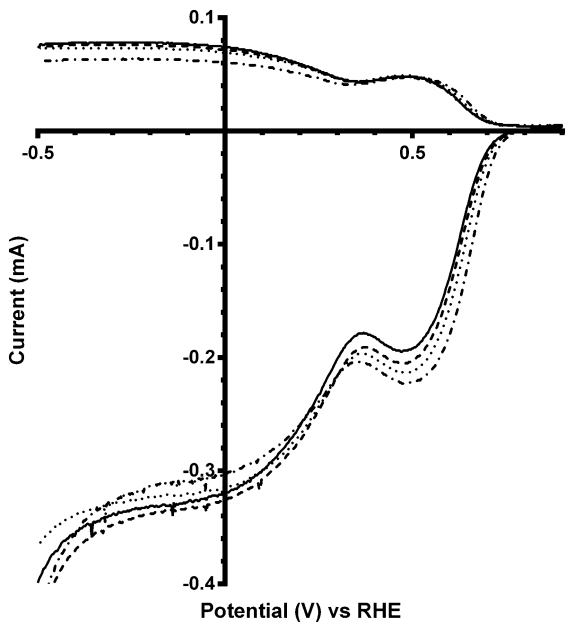

Fig. 10 RRDE LSVs of Ca_2RuBiO_6 in O_2-saturated aqueous KOH (1 mol dm^{-3}) and varying concentrations of K_2CO_3 at 600 rpm: solid line = K_2CO_3-free, dashed = 0.01 mol dm^{-3}, dotted = 0.05 mol dm^{-3}, and dash-dot = 0.1 mol dm^{-3}.

Table 6 Average n values and peroxide yields for Ca_2RuBiO_6 in O_2-saturated aqueous KOH (1 mol dm^{-3}) containing different concentrations of K_2CO_3[a]

Concentration of K_2CO_3/mol dm^{-3}	n_{RRDE}	Peroxide yield (%) from RRDE	n_{K-L}
0	2.57 ± 0.04	71.5 ± 2.1	2.96
0.01	2.62 ± 0.04	69.0 ± 1.7	3.12
0.05	2.61 ± 0.02	69.7 ± 1.2	2.92
0.1	2.73 ± 0.04	63.4 ± 2.1	3.06

[a] See footnotes to Table 2 for assumptions and the definition of errors.

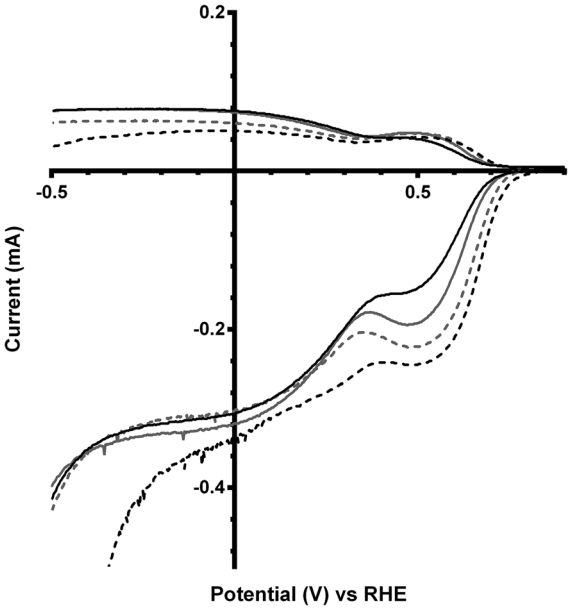

Fig. 11 RRDE LSVs of $Ca_2Ru_{2-x}Bi_xO_{7-y}$ ($x = 0.75$ in black, $x = 1$ in grey) in O_2-saturated aqueous KOH (1 mol dm^{-3}) containing the following concentrations of K_2CO_3: solid line = 0 mol dm^{-3} (CO_3^{2-}-free baseline) and dashed = 0.1 mol dm^{-3}. Rotation rate = 600 rpm.

doped catalysts (Fig. 9). However, the improved on-set potentials for the $x = 0.5$ and $x = 0.75$ Bi-doped catalysts in the presence of CO_3^{2-} are still less positive than those of the Bi-free parent catalyst in CO_3^{2-}-free electrolyte: the n values are all lower as well.

The final catalyst studied was the $x = 1$ sample (that contains significant levels of impurities). Again the on-set potentials shifted to more positive potentials, and the n values only slightly increased, on addition of CO_3^{2-} (Fig. 10 and Table 6). Interestingly, the on-set potential is better than the previous $Ca_2Ru_{1.25}Bi_{0.75}O_{6.25}$ catalyst in the CO_3^{2-}-free electrolyte (Fig. 11). However, interferences due to the Bi_2O_3 impurities cannot obviously be ruled out. Hence, a control experiment with Bi_2O_3 was conducted. This control experiment showed that Bi_2O_3 had a better on-set potential than the doped pyrochlore catalyst (Fig. 12): the increased on-set potential of the Ca_2RuBiO_6 catalyst (compared to $Ca_2Ru_{1.25}Bi_{0.75}O_{6.25}$) may well arise from the Bi_2O_3 impurities. However when CO_3^{2-} was added to the electrolyte the on-set potential of the Bi_2O_3 control

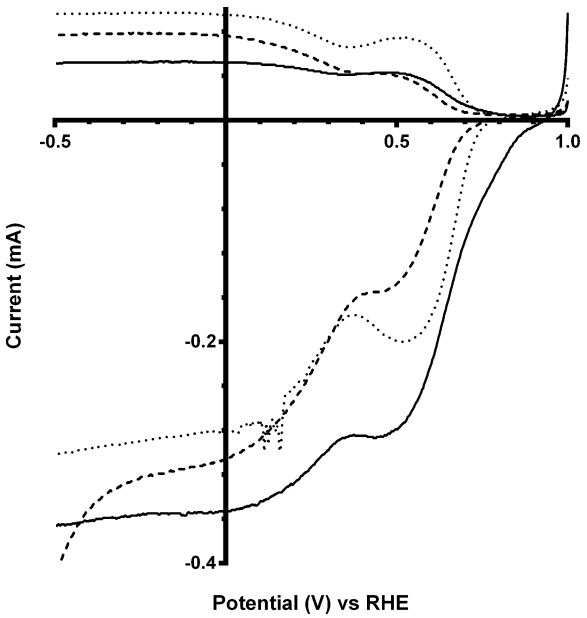

Fig. 12 RRDE LSVs of $Ca_2Ru_{2-x}Bi_xO_{7-y}$ ($x = 0$ solid line, $x = 0.75$ dashed line) and Bi_2O_3 (dotted line) in O_2-saturated aqueous KOH (1 mol dm^{-3}). Rotation rate = 600 rpm.

catalyst undesirably shifted to less positive potentials (not shown): this may explain why the improvement of on-set potential is less for the $x = 1$ catalyst compared to the $x = 0.75$ catalyst on addition of CO_3^{2-}.

Due to the $Ca_2Ru_{1.25}Bi_{0.75}O_{6.25}$ catalyst having the best response on addition of CO_3^{2-} (and the most well defined powder XRD profile with the lease amount of impurities), it was

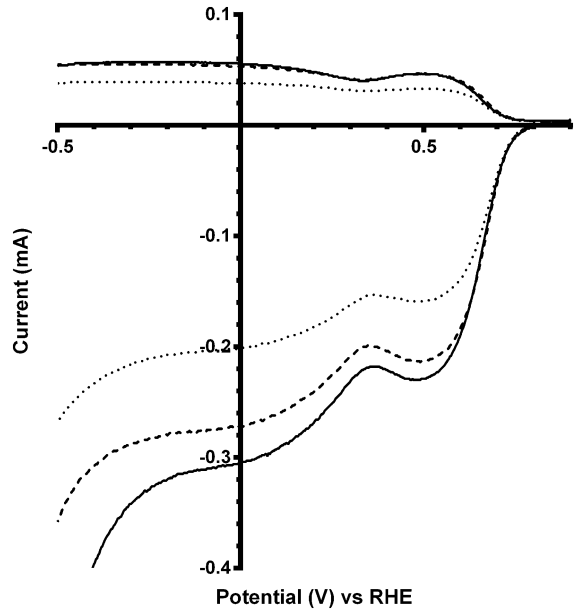

Fig. 13 RRDE LSVs of the $Ca_2Ru_{1.25}Bi_{0.75}O_{6.25}$ catalyst in O_2-saturated aqueous KOH (1 mol dm^{-3}) and varying concentrations of K_2CO_3 at 600 rpm: solid line = 0.1 mol dm^{-3}, dashed = 0.2 mol dm^{-3}, and dotted = 0.5 mol dm^{-3}.

decided to investigate the addition of even greater concentrations of K_2CO_3. On an increase to 0.5 mol dm^{-3}, the on-set potential and n value did not vary significantly compared to the K_2CO_3 (0.1 mol dm^{-3}) electrolyte. However there was a significant decrease in current in the diffusion limited region. This indicates significant changes in the properties of the solution and a lowering of the diffusion limited current defined by the Levich equation (eqn (6)):[21,22]

$$i_L = 0.62nFAD_o^{2/3}\omega^{1/2}\nu^{-1/6}C_o \quad (6)$$

As well as changing the ionic strength and pH of the solutions (which is why a RHE was used: the measured potentials using a Gaskatel RHE do not change with pH [unlike with the use of other hydrogen-based reference electrodes]), the addition of salts to the electrolyte can cause a decrease in both the O_2 concentration and the diffusion coefficient. In conjunction with the rise in kinematic viscosity, this reduces the limiting current of the system. To determine whether the on-set potentials may be significantly affected by addition of too high a concentration of K_2CO_3, a lower concentration of 0.2 mol dm^{-3} was additionally tested. Again the on-set potential did not vary significantly, while the limiting current was intermediate between the 0.1 and 0.5 mol dm^{-3} K_2CO_3 tests (Fig. 13).

As seen in the Tables of data presented, the e^- n value can also been calculated using the Koutecký–Levich equation (eqn (7) – a modified version of eqn (6):

$$n = (1/\text{slope})/0.62FD^{2/3}\nu^{-1/6}C_oA \quad (7)$$

where n = number of electrons, F = Faraday Constant (96 485 C mol^{-1}), D = the O_2 diffusion coefficient (taken here as = 2.04×10^{-5} cm^2 s^{-1}), ν = kinematic viscosity (taken here as = 0.01 cm^2 s^{-1}), C_o = bulk concentration of O_2 (taken here as = 7.8×10^{-7} mol cm^{-3}), A = disk area (0.2475 cm^2), and the gradient of the slopes are from the plots in Fig. 14 (for the $Ca_2Ru_{1.75}Bi_{0.75}O_{6.25}$ catalyst).

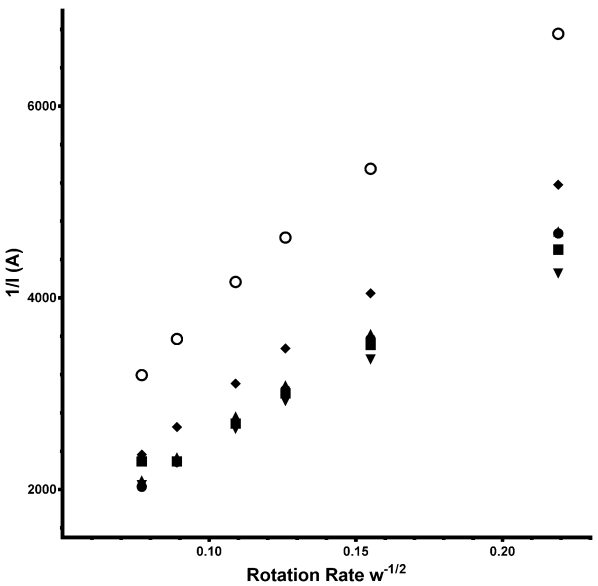

Fig. 14 Koutecký–Levich plots for $Ca_2Ru_{1.25}Bi_{0.75}O_{6.26}$ in aqueous KOH (1 mol dm^{-3}) containing varying concentrations of K_2CO_3: filled circle = K_2CO_3-free (baseline), square = 0.01 mol dm^{-3}, triangle = 0.05 mol dm^{-3}, inverted triangle = 0.1 mol dm^{-3}, diamond = 0.2 mol dm^{-3} and circle = 0.5 mol dm^{-3}.

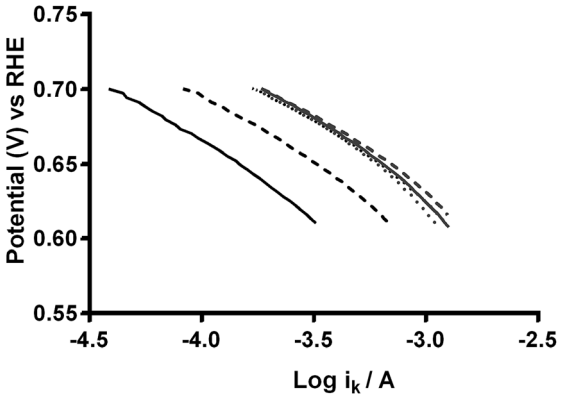

Fig. 15 Tafel plots of the $Ca_2Ru_{1.25}Bi_{0.75}O_{6.25}$ catalyst in O_2-saturated aqueous KOH (1 mol dm^{-3}) with varying concentrations of K_2CO_3: black solid = K_2CO_3-free, black dashed = 0.01 mol dm^{-3}, black dotted = 0.05 mol dm^{-3}, grey solid = 0.1 mol dm^{-3}, grey dashed = 0.2 mol dm^{-3}, and grey dotted = 0.5 mol dm^{-3}.

As stated earlier, the values for the various electrolyte parameters (*e.g.* O_2 concentration *etc.*) are incorrect when K_2CO_3 is added to the electrolyte (more so with high concentrations): however, this shouldn't affect the values for the K_2CO_3-free aqueous KOH (1 mol dm^{-3}) electrolyte (where the above values are well established). The reason for the discrepancies between the n values determined from the RRDE method (ratio of ring to disk currents) and K–L analyses may arise from the area A used in eqn (6) and (7). The A used in the calculation is the area of the GC-disk but the powdered catalyst will not fully cover the GC-disk and will cause other uncertainties in A as the catalyst layers will not flat when deposited: hence, the A values

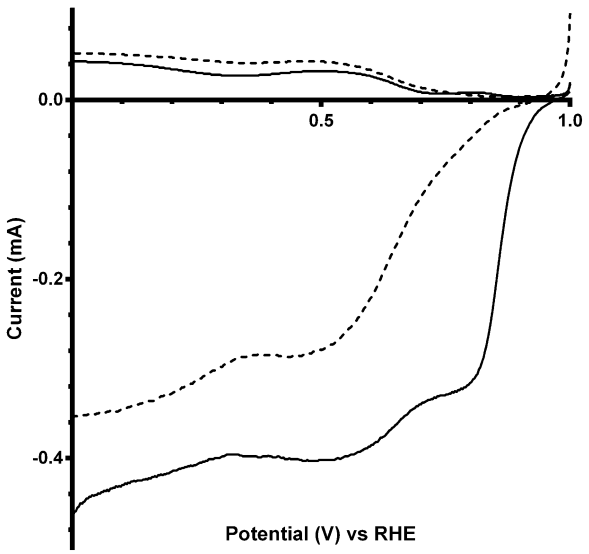

Fig. 16 RRDE LSV comparison of $Ca_2Ru_2O_7$ (dashed) and Pt black (solid) in O_2-saturated KOH (1 mol dm^{-3}) at 600 rpm.

Table 7 Average n values and peroxide yields in O_2-saturated K_2CO_3-free aqueous KOH (1 mol dm^{-3})[a]

Catalyst	n_{RRDE}	Peroxide yield (%) from RRDE	n_{K-L}
$Ca_2Ru_2O_7$	2.97 ± 0.02	51.3 ± 1.0	2.14
$Ca_2Ru_{1.25}Bi_{0.75}O_{6.25}$	2.55 ± 0.02	72.7 ± 1.1	2.95
Pt black	3.33 ± 0.03	33.4 ± 1.6	3.28

[a] See footnotes to Table 2 for assumptions and meaning of errors.

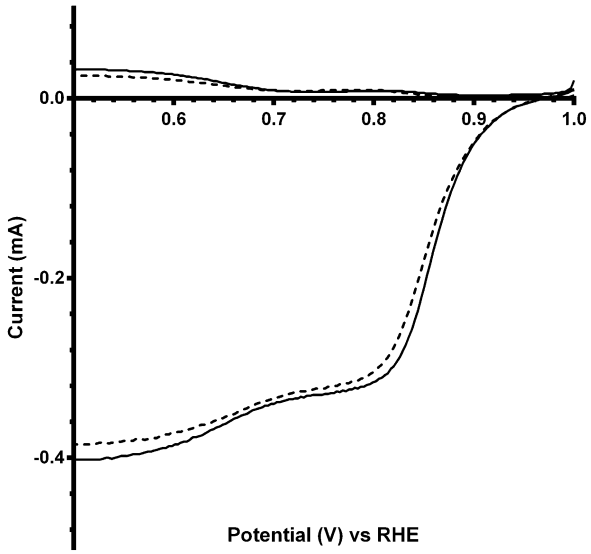

Fig. 17 RRDE LSVs of Pt black catalyst in O_2-saturated aqueous KOH (1 mol dm^{-3}) containing the following concentrations of K_2CO_3: solid line = 0 mol dm^{-3} (CO_3^{2-}-free baseline) and dashed = 0.1 mol dm^{-3}. Rotation rate = 600 rpm.

will be different for each catalyst with undetermined uncertainties and errors (which is why the RRDE is a preferred method for analysing the response with such catalysts). Further analysis of the data involved the Tafel plots for $Ca_2Ru_{1.25}Bi_{0.75}O_{6.25}$ in O_2-saturated aqueous KOH (1 mol dm^{-3}) with different concentrations of K_2CO_3 (see Fig. 15).[23] The Tafel slopes for all concentrations of CO_3^{2-} are similar. Interestingly, the curves are desirably shifted to the right with increasing concentrations of CO_3^{2-} (with a plateau at 0.1 mol dm^{-3}). This suggests that either the presence of CO_3^{2-} enhances the ORR kinetics or that the mechanism or reaction occurring has changed.

Additional experiments were performed on a Pt black catalyst to compare with the parent pyrochlore catalyst. As seen in Fig. 16 the Pt black performs better than the $Ca_2Ru_2O_7$ in both on-set potential and electron transfer number (Table 7) with the CO_3^{2-}-free electrolyte. On the addition of the CO_3^{2-} the electrolyte the on-set potential of the Pt black catalyst decreases (Fig. 17): however, the on-set potential is still significantly greater than that of those of the pyrochlore catalysts. This poorer performance in CO_3^{2-}-containing solution compared to the CO_3^{2-}-free solution is also seen with Tafel plots for Pt black

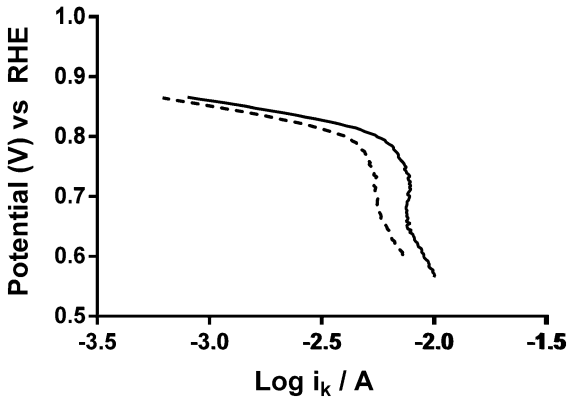

Fig. 18 Tafel plots of Pt black in O_2-saturated aqueous KOH (1 mol dm^{-3}) with varying concentrations of K_2CO_3: solid = K_2CO_3-free and dashed = 0.1 mol dm^{-3}.

(Fig. 18): the CO_3^{2-}-free electrolyte gives higher ORR kinetic performances and confirms the prior work by Vega *et al.*[1]

Conclusions

The *ex situ* oxygen reduction reaction (ORR) activity of $Ca_2Ru_{2-x}Bi_xO_{7-y}$ (x = 0, 0.25, 0.5, 0.75 and 1) pyrochlore catalysts were investigated, in aqueous KOH (1 mol dm^{-3}) electrolytes in both the absence and presence of K_2CO_3, using rotating ring disk electrode (RRDE) studies. The synthesis of the $x = 1$ example was less successful than the others with significant levels of Bi_2O_3 impurities (electroactive in its own right). The additional of CO_3^{2-} to the electrolyte generally improved the electrode kinetics of the pyrochlore catalysts and gave more positive on-set potentials (compared to the CO_3^{2-}-free electrolytes), especially with higher levels Bi-doping (*e.g.* the $x = 0.75$ example). There was a significant decrease in the on-set potentials (shift to less positive values) for the pyrochlore catalysts compared to a Pt black benchmark even with the addition of CO_3^{2-} into the system. All pyrochlore catalysts gave higher peroxide yields compared to the Pt black benchmark catalyst: peroxide yields were higher with the Bi-doped catalysts compared to the Bi-free pyrochlore parent catalyst.

This *ex situ* study shows that such $Ca_2Ru_{2-x}Bi_xO_{7-y}$ pyrochlore catalysts have unusual ORR behaviours in aqueous alkali electrolytes in the presence of CO_3^{2-} anions and this warrants further fundamental studies. Future studies should also investigate the *in situ* performances of the catalysts in fuel cells with an O_2(air)/CO_2 mix feeds at the cathode further probe the properties of the catalyst and to investigate if such catalysts operate *via* carbonate cycles in low temperature carbonate fuel cells containing anion-exchange membranes.

Acknowledgements

The authors like to thank the UK's Engineering & Physical Sciences Research Council (EPSRC) for funding grant EP/I004882/1. The IviumStat bipotentiostat used was purchased

using funding from EPSRC grant EP/H019480/1 (SuperGen Biological Fuel Cells consortium).

References

1 J. A. Vega and W. E. Mustain, *Electrochim. Acta*, 2010, **55**, 1638.
2 J. A. Vega, S. Shrestha, M. Ignatowich and W. E. Mustain, *J. Electrochem. Soc.*, 2012, **159**, B12.
3 J. A. Vega, C. Chartier and W. E. Mustain, *J. Power Sources*, 2010, **195**, 7176.
4 J. A. Vega, S. Smith and W. E. Mustain, *J. Electrochem. Soc.*, 2011, **158**, B349.
5 M. Unlu, J. Zhou and P. Kohl, *Electrochem. Solid-State Lett.*, 2009, **12**, B27.
6 L. Demarconnay, C. Coutanceau and J. M. Leger, *Electrochim. Acta*, 2004, **49**, 4513.
7 V. Rao, Hariyanto, C. Cremers and U. Stimming, *Fuel Cells*, 2007, **7**, 417.
8 (*a*) K.-D. Kreuer, *Chem. Mater.*, 2014, **26**, 361; (*b*) M. A. Hickner, A. M. Herring and E. B. Coughlin, *J. Polym. Sci., Part B: Polym. Phys.*, 2013, **51**, 1727; (*c*) J. Pan, C. Chen, L. Zhuang and J. Lu, *Acc. Chem. Res.*, 2012, **45**, 473; (*d*) G. Merle, M. Wessling and K. Nijmeijer, *J. Membr. Sci.*, 2011, **377**, 1; (*e*) R. Zeng and J. R. Varcoe, *Recent Pat. Chem. Eng.*, 2011, **4**, 93; (*f*) J. R. Varcoe, J. P. Kizewski, D. M. Halepoto, S. D. Poynton, R. C. T. Slade and F. Zhao, in *Encyclopedia of Electrochemical Power Sources*, ed. J. Garche, C. Dyer, P. Moseley, Z. Ogumi, D. Rand and B. Scrosati, Elsevier, Amsterdam, 2009, vol. 2, pp. 329–343; (*g*) R. C. T. Slade and J. R. Varcoe, *Fuel Cells*, 2005, **5**, 187; (*h*) T. Xu, *J. Membr. Sci.*, 2005, **263**, 1.
9 N. Li, M. D. Guiver and W. H. Binder, *ChemSusChem*, 2013, **6**, 1376.
10 H. Long, K. Kim and B. S. Pivovar, *J. Phys. Chem. C*, 2012, **116**, 9419.
11 C. M. Lang, K. Kim and P. Kohl, *Electrochem. Solid-State Lett.*, 2006, **9**, A545.
12 N. S. Spinner, J. A. Vega and W. E. Mustain, *Catal. Sci. Technol.*, 2012, **2**, 19.
13 J. A. Vega, N. Spinner, M. Catanese and W. E. Mustain, *J. Electrochem. Soc.*, 2012, **159**, B19.
14 J. Prakash, D. A. Tryk, W. Aldred and E. B. Yeager, *J. Appl. Electrochem.*, 1999, **29**, 1463.
15 J. Prakash, D. A. Tryk and E. B. Yeager, *J. Electrochem. Soc.*, 1999, **146**, 4145.
16 L. Yao, D. Wang, W. Peng, W. Hu, H. Yuan and S. Feng, *Sci. China: Chem.*, 2011, **54**, 941.
17 T. Munenaka and H. Sato, *J. Phys. Soc. Jpn.*, 2006, **75**, 103801.
18 G. Haranyi, *J. Solid State Electrochem.*, 1998, **2**, 237.
19 C. A. Hancock, A. Ong and J. R. Varcoe, *J. Mater. Chem. A*, 2014, **2**, 3047.
20 J. Sunarso, A. A. J. Torriero, W. Zhou, P. C. Howlett and M. Forsyth, *J. Phys. Chem. C*, 2012, **116**, 5827.
21 S. Treimer, A. Tang and D. C. Johnson, *Electroanalysis*, 2002, **14**, 165.
22 C. H. Hamann, A. Hamnett and W. Vielstich, *Electrochemistry*, Wiley-VCH, Germany, 2nd edn, 2007, pp. 193–197.
23 E. Gileadi, *Physical Electrochemistry Fundamentals, Techniques and Applications*, Wiley-VCH, Germany, 2011, p. 65.